Optimizing the Metal Binding Parameters of an EF-Hand-Like Calcium Chelation Loop: Coordinating Side Chains Play a More Important Tuning Role than Chelation Loop Flexibility†

Steven K. Drake, Michael A. Zimmer, Cory L. Miller, and Joseph J. Falke*

Department of Chemistry and Biochemistry, University of Colorado, Boulder, Colorado 80309-0215

Received February 20, 1997; Revised Manuscript Received May 19, 1997⊗

ABSTRACT: In calcium signaling pathways regulated by the EF-hand Ca^{2+} binding motif, proper regulation requires that the equilibrium and kinetics of Ca^{2+} binding to the EF-hand chelation loop be precisely optimized for each physiological application. Studies of small-molecule organic chelators have shown that metal binding parameters can be tuned both by the nature of the coordinating ligands and by the structural framework to which these ligands are attached. By analogy, the present study tests the relative importance of (i) coordinating side chains and (ii) backbone torsion angle constraints to the tuning of an EF-hand-like Ca^{2+} chelation loop. A series of engineered chelation loops are generated by modifying Ca^{2+} binding site of the *Escherichia coli* galactose binding protein. The resulting loops, each containing an altered coordinating side chain or a Gly substitution, are compared with respect to their metal binding affinities, specificities, and dissociation kinetics. The Gly variants examined include substitutions which eliminate or introduce a Gly at each of the nine chelation loop positions. The results reveal that Gly is not tolerated at loop positions 1, 3, 5, or 8 or at the external coordinating position, where the removal of a key coordinating or hydrophobic side chain destabilizes the protein. In contrast, Gly residues at loop positions 2, 4, 6, and 7, none of which is required for side chain coordination, have little effect on Ca^{2+} affinity and the ability to discriminate between cations of different size and charge. Kinetic measurements show that some of these Gly residues measurably alter the rates of metal ion association and dissociation, but in each case the two rates are changed by approximately the same factor so that the effects on equilibrium are minor. Overall, Gly residues yield surprisingly small effects at loop positions 2, 4, 6, and 7, especially when compared to the larger equilibrium and kinetic effects observed for coordinating side chain substitutions. It follows that the conserved Gly at position 6 is not required for Ca^{2+} binding and that constraints on the backbone torsion angles at the non-coordinating side chain positions 2, 4, 6, and 7 play a relatively minor role in tuning metal binding parameters. Instead, specific coordinating side chains optimize the metal binding parameters of the GBP chelation loop for its protein context and biological application.

The EF-hand Ca^{2+} binding motif is widely used in nature where its functions include Ca^{2+} signaling, buffering, and structural stabilization [reviewed by Linse and Forsén (1995), Falke et al. (1994), Kawasaki and Kretsinger (1994), Skelton et al. (1994), Marsden et al. (1990), and Strynadka and James (1989)]. Over 1000 EF-hand sites have already been identified in protein primary structures (Kawasaki & Kretsinger, 1994). The structure of the EF-hand motif consists of a Ca^{2+} chelation loop which bridges two α-helices, one at each end, yielding a helix−loop−helix structural unit. In general, two helix−loop−helix units exist in the same protein and associate to form a distinct domain containing two Ca^{2+} binding sites. Within this domain each of the two Ca^{2+} chelation loops, termed the EF-loops, provide five coordinating positions stabilizing the bound Ca^{2+} ion, while a sixth coordinating position is located outside each loop as illustrated in Figure 1 and Table 1. Although different EF-hand sites share the same general architecture, their detailed structures can be highly specialized for different proteins and functions, yielding greatly varying Ca^{2+} binding parameters. As a result, the Ca^{2+} binding affinity, selectivity, and kinetics are observed to vary over 3 orders of magnitude among the EF-hand proteins characterized thus far (Linse & Forsén, 1995; Falke et al., 1994). Simple molecular principles appear to underlie such tuning, and many of the same principles are likely to be relevant to other Ca^{2+} binding motifs, for instance, those of Ca^{2+} channels and pumps (Chen et al., 1996; Carafoli et al., 1996; Miller, 1996; Park & MacKinnon, 1995). In EF-hand proteins molecular tuning is provided by (i) specific features of the EF-loop, (ii) the context of the protein outside the EF-loop, and (iii) intermolecular interactions with effector proteins (Peersen et al., 1997; Linse & Forsén, 1995; Falke et al., 1994). In principle, the intra-loop component of tuning could be dominated by specific coordinating side chains, or by constraints on the backbone structure of the loop. Currently the relative contributions of side chain and backbone constraints to intra-loop tuning are unknown because a systematic study of the effects of backbone constraints on ion binding parameters has not yet been carried out.

Because Gly lacks a side chain, it provides a larger range of backbone torsion angles than any other amino acid. Even the most conservative replacement, Ala, is more strictly

† Support Provided by NIH Grant GM48203.

* Corresponding author. Tel: (303) 492-3503. FAX: (303) 492-5894. E-mail: falke@colorado.edu.

⊗ Abstract published in *Advance ACS Abstracts,* July 1, 1997.

S0006-2960(97)00391-7 CCC: $14.00

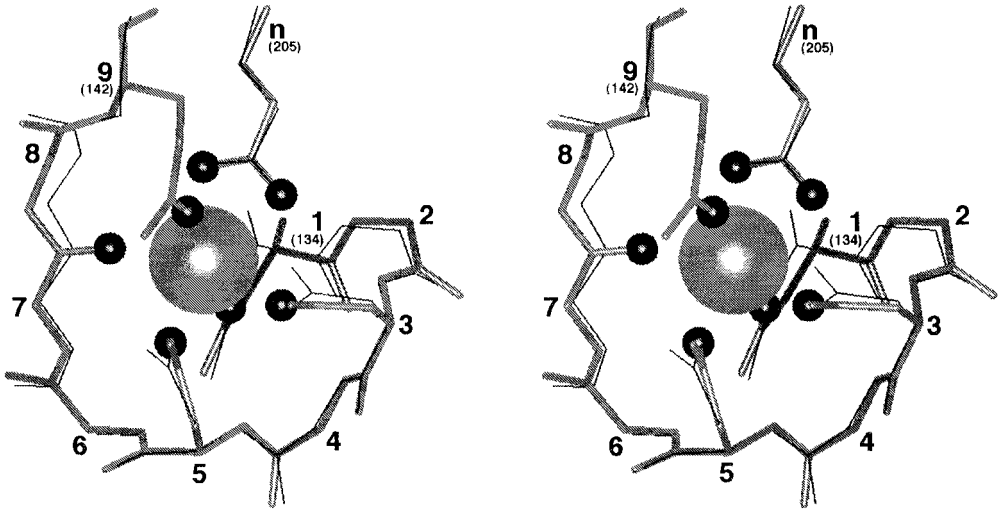

FIGURE 1: Stereodiagram of the GBP Ca^{2+} binding site (cylindrical bonds) superimposed on EF-hand site IV of human calmodulin (fine bonds). Both sites illustrate the standard conformation of the nine-residue Ca^{2+} binding loop as well as the typical disposition of the conserved Glu side chain (n) outside the loop (Vyas et al., 1987; Chattopadhyaya et al., 1992). Also shown for the GBP site are bound Ca^{2+} (large sphere) and the seven coordinating oxygens (dark spheres). The major difference between the two loops is the coordination at the axial ninth loop position. GBP, like certain eukaryotic EF-hand sites, provides direct side chain coordination at this position (Gln142). In contrast, site IV of calmodulin, like many other EF-hand sites, utilizes a coordinating solvent oxygen at this position (not shown).

Table 1: Frequency of Gly at EF-Loop Positions in Natural EF-Hand Sites

	EF-loop position[a]									
	1	2	**3**	4	**5**	6	**7**	8	**9**	**external** (n)
Gly										
all sites[b]	1.4%	1.5%	4.2%	43.1%	2.9%	73.6%	1.1%	0.0%	6.8%	0.3%
classical sites[c]	NA	0.2%	NA	55.3%	1.2%	94.2%	NA	NA	8.7%	NA
Classical residues[c]	D	X	D N S	(I) (L) (V) (F) (Y) (W)	D S N T G E	G N D K R H Q	(G) (P)	I V L M C	D S T E N G Q C A	E D
GBP site[d]	D	L	N	K	D	G	Q	I	Q	E

[a] Coordinating positions are shown in bold. [b] Database of 1073 aligned EF-loop sequences courtesy of Dr. R. H. Kretsinger (Kawasaki & Kretsinger, 1994). [c] Classical sites defined by the Prosite algorithm, as previously described (Falke et al., 1994). NA = Gly is not allowed; X = all residues are allowed; (Z) = residue Z is not allowed. [d] Sequence of the wild type GBP site (Vyas et al., 1987).

limited in the allowed ϕ,ψ angles, as Figures 2A and B illustrate. Figure 2C also summarizes the backbone ϕ,ψ angles for the nine positions of the EF-loop, derived from the crystal structures of 45 Ca^{2+}-occupied sites (Falke et al., 1994). Of particular interest are EF-loop positions 4 and 6, which display torsion angles similar to those of a left-handed α-helix, falling within a region of ϕ,ψ space more heavily populated by Gly than any other amino acid (compare Figures 2A and C). Not surprisingly, Gly is prevalent at these positions in natural EF-hand sites, as illustrated in Table 1. Examination of the current database of 1073 aligned EF-loops (Kawasaki & Kretsinger, 1994) reveals that Gly occurs at frequencies of 43%, 74%, and 7% at positions 4, 6, and 9, respectively, while its frequency is under 5% at all other positions. These same three positions exhibit even higher Gly frequencies of 55%, 94%, and 9%, respectively, in the "classical" subset of EF-loops which share features characteristic of known high-affinity Ca^{2+} binding sites (Falke et al., 1994).

A priori, one might expect that the ion binding parameters of the EF-loop could be highly sensitive to internal Gly substitutions. In organic chelators, for example, the stabilizing effect of chelation is maximal when a constrained structural framework positions the coordinating moieties at locations compatible with metal binding [Schwarzenbach, 1952; reviewed in Falke et al. (1994)]. Previous studies have examined the role of EF-loop backbone flexibility by substituting Gly at two of the nine EF-loop positions. It was found that Gly incorporation at the fourth EF-loop position had little or no effect on metal binding affinity, selectivity, or kinetics (Drake et al., 1996; Drake & Falke, 1996; DaSilva et al., 1995). A separate study revealed that Gly incorporation at the ninth EF-loop position, also termed the gateway position, yielded altered metal on- and off-rates due primarily to the removal of the gateway side chain rather than to reduced constraints on backbone torsion angles (Drake et al., 1996; Drake & Falke, 1996). In order to fully ascertain the tuning contribution of EF-loop backbone flexibility, however, it is necessary to examine the effects of altered torsion angle constraints at all nine loop positions.

Here, we incorporate or remove Gly at each of the loop positions, enabling direct comparison of the resulting per-

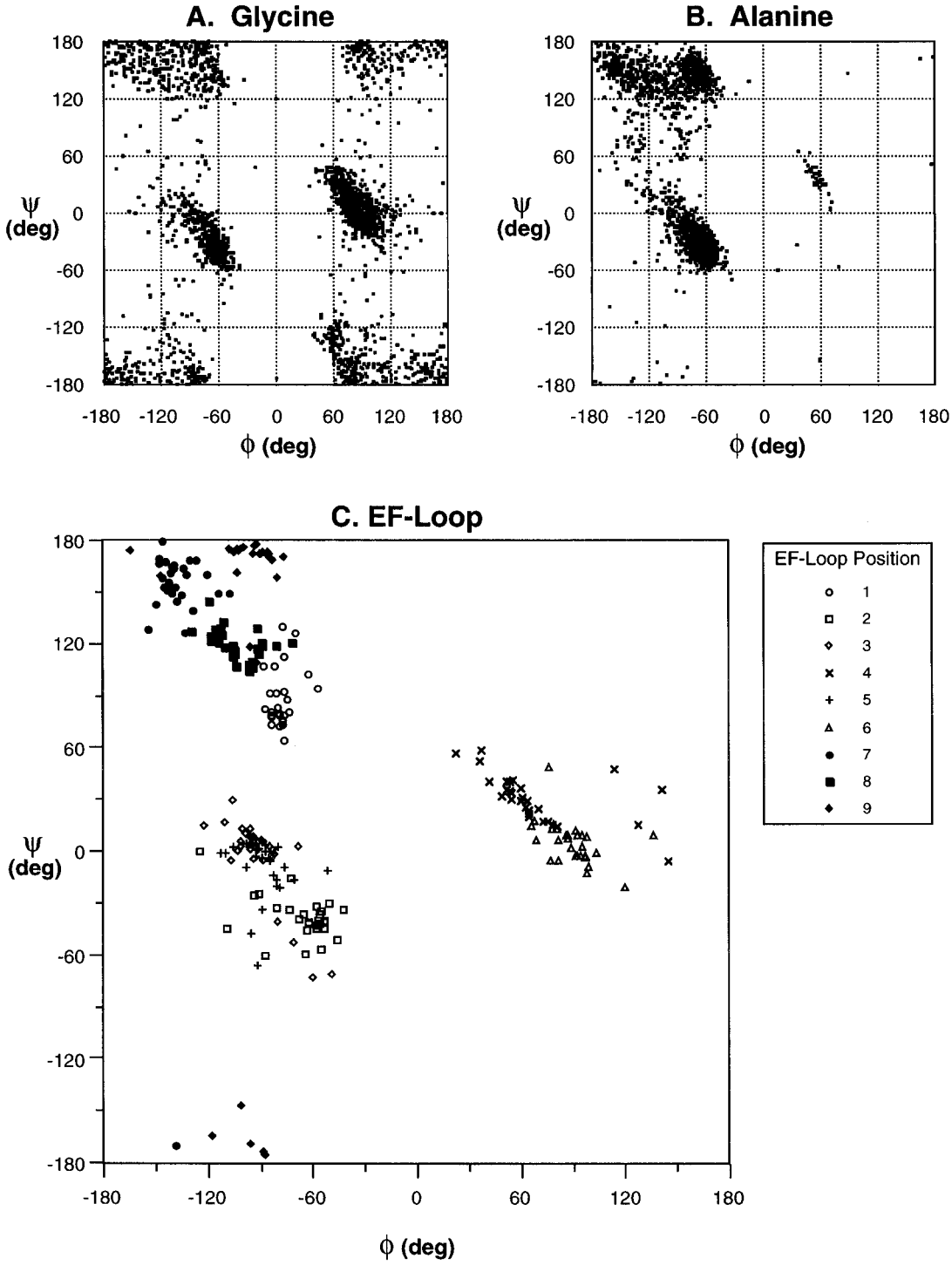

FIGURE 2: Ramachandran ϕ,ψ distributions for Gly, Ala, and the EF-loop. The backbone ϕ,ψ angles of 137 non-homologous protein crystal structures (Brookhaven Protein Data Bank) were analyzed to generate the illustrated distributions for (A) Gly (2493 residues) and (B) Ala (2539 residues). These can be compared to (C), which displays the ϕ,ψ angles observed for each of the nine EF-loop positions in 45 crystal structures of Ca^{2+}-occupied sites (Falke et al., 1994).

turbations with those generated by a series of non-Gly control mutations at coordinating side chain positions 3 and 9. The Gly substitutions (i) alter the loop thermal dynamics or entropy, (ii) modulate its range of motion or pliability, or (iii) remove specific side chain interactions. Such modifications of the loop conformation or entropy would be expected to change the affinity of metal binding, while the modified loop dynamics could modulate the kinetics of metal binding and release. Finally, the stiffness of the loop toward expansion and contraction could control its ability to discriminate between metal ions of different size.

Our study uses the Ca^{2+} chelation loop of the *Escherichia coli* galactose binding protein (GBP) as a model for the EF-loop of eukaryotic EF-hand proteins. The GBP Ca^{2+} binding site, which stabilizes the folded structure of GBP, differs from the EF-hand motif in that its Ca^{2+} chelation loop links an α-helix and a β-strand rather than two α-helices. In addition, the coordinating bidentate Glu outside the loop lies 63 residues, rather than the standard three residues, beyond the loop C-terminus: such an arrangement is important to GBP structural stabilization since it allows the Ca^{2+} ion to

bridge distal regions of the protein sequence. However, the backbone and coordination structures of the GBP Ca^{2+} chelation loop, as well as the spatial location of the external bidentate Glu side chain, all fall within the range of structures observed for standard EF-hand sites. Figure 1 illustrates this similarity by superimposing the backbone structure of the GBP Ca^{2+} binding loop and that of EF-hand site IV of human calmodulin. Experimentally, the EF-loop of GBP is well-suited for studies analyzing the effects of intra-loop substitutions on metal binding, since a sensitive fluorescence assay for metal binding to the site has been described (Snyder et al., 1990) and the single-site nature of the GBP system facilitates the quantitation of metal binding parameters.

For the present study, Gly substitutions were generated at all nine positions of the GBP model EF-loop, as well as at the external coordinating position. Some Gly substitutions destabilized the protein and blocked expression, but most yielded stable proteins which were isolated and characterized with respect to their affinities for Ca^{2+} and 19 other spherical metal ions. The metal dissociation kinetics of each site were also measured. Gly substitutions at non-coordinating positions yield surprisingly minor effects, with the exception of a Gly substitution for the essential hydrophobic residue at loop position 8. In contrast, both Gly and non-Gly substitutions at coordinating side chain positions have significantly larger effects on metal binding parameters. Overall, the observed results, together with an analysis of natural EF-loop sequences, suggest that coordinating side chains rather than Gly residues serve to specialize the Ca^{2+} binding parameters of the GBP EF-loop for its structural and biological contexts.

METHODS

Protein Engineering, Purification, and Characterization. GBP substitutions were engineered via Kunkel-based site-directed mutagenesis and confirmed by plasmid DNA sequencing, as previously described (Drake & Falke, 1996; Falke et al., 1991). Protein expression was screened by growth of plasmid-bearing *E. coli* in standard media containing 1 mM each of added $MgCl_2$, $CaCl_2$, and $SrCl_2$ followed by analysis on SDS−PAGE (Drake & Falke, 1996). Mutants were deemed non-expressers if they yielded expression levels ≤5% that of wild type, as quantitated by gel scans of Coomassie-stained bands. The remaining viable mutants were expressed and purified by a standard procedure, and their masses were measured by a Sciex API-III triple-quadropole electrospray mass spectrometer to confirm that each protein contained only the desired single-point mutation (Drake & Falke, 1996). Thermal melting curves and galactose binding assays were used to characterize the protein stability and functionality, respectively, as detailed elsewhere (Drake & Falke, 1996).

Ion Affinities and Dissociation Rates. Equilibrium binding of Tb^{3+}, as well as Tb^{3+} dissociation upon rapid mixing with excess EDTA, was measured by a fluorescence energy transfer assay as previously described (Drake & Falke, 1996; Drake et al., 1996). The binding affinities of other metal ions were determined by competition with Tb^{3+} in the same assay (Drake et al., 1996). Metal binding affinities were expressed either as equilibrium dissociation constants (K_D) or as binding free energies ($\Delta G_B^\circ = RT \ln K_D$). All fluorescence measurements utilized an SLM 48000S spectrofluoroimeter equipped with a stopped-flow attachment.

Comparison of Binding Free Energies: Theory. A general reaction scheme that describes the present study compares the binding of metals M_a and M_b to proteins P and P′, respectively:

$$M_a(aq) \xrightarrow{\Delta G_{M_a}^\circ} M_a \quad (1a)$$

$$P{\cdot}W_x{\cdot}H^+_u + M_a \xrightarrow{\Delta G_a^\circ} P^*{\cdot}M_a{\cdot}W_y{\cdot}H^+_v + \Delta W + \Delta H^+ \quad (1b)$$

$$M_b(aq) \xrightarrow{\Delta G_{M_b}^\circ} M_b \quad (2a)$$

$$P'{\cdot}W'_x{\cdot}H^{+\prime}_u + M_b \xrightarrow{\Delta G_b^\circ} P'^*{\cdot}M_b{\cdot}W'_y{\cdot}H^{+\prime}_v + \Delta W' + \Delta H^{+\prime} \quad (2b)$$

Each binding reaction begins with the dehydration of the aqueous metal ion ($M_a(aq)$ or $M_b(aq)$) to yield the bare metal ion (M_a or M_b); for this step the dehydration free energy is known for each of the metal ions used in this study, ranging from +62 to +908 kcal mol^{-1} for Cs^+ and Sc^{3+}, respectively. The second step of each reaction represents the binding of the bare metal ion (M_a or M_b) to the hydrated and protonated apo-protein ($P{\cdot}W_x{\cdot}H^+_u$ or $P'{\cdot}W'_x{\cdot}H^{+\prime}_u$), where the products are the metal-occupied protein ($P^*{\cdot}M_a{\cdot}W_y{\cdot}H^+_v$ or $P'^*{\cdot}M_b{\cdot}W'_y{\cdot}H^{+\prime}_v$) and the freed water molecules (ΔW or $\Delta W'$) and protons (ΔH^+ or $\Delta H^{+\prime}$). The asterisk indicates possible changes to the protein conformation or dynamics upon metal binding.

The difference in the binding free energies of the two overall reactions indicated by eqs 1 and 2 ($\Delta\Delta G_B^\circ$) can be expressed in terms of the metal ion dehydration free energies ($\Delta G_{M_a}^\circ - \Delta G_{M_b}^\circ$), together with the free energies of formation for the remaining reactants and products ($\Delta G_a^\circ - \Delta G_b^\circ$), as given by

$$\begin{aligned}\Delta\Delta G_B^\circ &= [\Delta G_{M_a}^\circ - \Delta G_{M_b}^\circ] \\ &+ [\Delta G_f^\circ(P^*{\cdot}M_a{\cdot}W_y{\cdot}H^+_v) - \Delta G_f^\circ(P'^*{\cdot}M_b{\cdot}W'_y{\cdot}H^{+\prime}_v)] \\ &+ [\Delta G_f^\circ(\Delta W) - \Delta G_f^\circ(\Delta W')] \\ &+ [\Delta G_f^\circ(\Delta H^+) - \Delta G_f^\circ(\Delta H^{+\prime})] \\ &- [\Delta G_f^\circ(P{\cdot}W_x{\cdot}H^+_u) - \Delta G_f^\circ(P'{\cdot}W'_x{\cdot}H^{+\prime}_u)] \\ &- [\Delta G_f^\circ(M_a) - \Delta G_f^\circ(M_b)] \\ &= \Delta\Delta G^\circ[\text{metal dehydration}] \\ &+ \Delta\Delta G_f^\circ[\text{metal-occupied protein}] \\ &+ \Delta\Delta G_f^\circ[\text{released water}] \\ &+ \Delta\Delta G_f^\circ[\text{released protons}] \\ &- \Delta\Delta G_f^\circ[\text{apo-protein}] \\ &- \Delta\Delta G_f^\circ[\text{bare metal}] \end{aligned} \quad (3)$$

Note that the free energies of formation for the bare metal ions make equal but opposite contributions in the terms {$+\Delta\Delta G_f^\circ$[metal-occupied protein]} and {$-\Delta\Delta G_f^\circ$[bare metal]} and thus do not contribute to the overall free energy difference. Moreover, eq 3 simplifies further for the two specific comparisons made in the present work. One type of comparison considers the binding of different metal ions to the same wild type or engineered site, in which case the

Table 2: Effects of Ca^{2+} Binding Loop Glycine Substitutions on Protein Stability and Sugar Binding

loop position	site	altered residue	change in volume[a] (Å^3)	expression	protein mass		T_m (±1 °C)	K_D(Gal) (μM)
					predicted (Da)	measured (±4 Da)		
	WT			+	33 368	33 370	58.5	0.5 ± 0.1
1	D134G	Asp	−43	−				
2	L135G	Leu	−76	+	33 312	33 310	52.3	0.38 ± 0.06
3	N136G	Asn	−48	−				
4	K137G	Lys	−87	+	33 299	33 298	58.1	0.6 ± 0.2
5	D138G	Asp	−43	−				
6	G139N	Gly	+48	+	33 425	33 425	57.1	0.15 ± 0.07
6/7	G139N/Q140G	Gly/Gln	−18	+	33 354	33 353	52.7	0.32 ± 0.06
7	Q140G	Gln	−66	+	33 297	33 297	56.3	0.14 ± 0.04
8	I141G	Ile	−76	−				
9	Q142G	Gln	−66	+	33 297	33 296	53.6	0.17 ± 0.03
n	E205G	Glu	−61	−				

[a] Creighton, 1993.

apo-protein is identical ($\Delta\Delta G_f^\circ$[apo-protein] = 0), yielding

$$\Delta\Delta G_B^\circ = \Delta\Delta G^\circ[\text{metal dehydration}] + \Delta\Delta G_f^\circ[\text{metal-occupied protein}] + \Delta\Delta G_f^\circ[\text{released water}] + \Delta\Delta G_f^\circ[\text{released protons}] - \Delta\Delta G_f^\circ[\text{bare metal}] \quad (4)$$

The other type of comparison considers the binding of the same metal ion to different sites, in which case the metal terms drop out ($\Delta\Delta G_f^\circ$[bare metal] = $\Delta\Delta G^\circ$[metal dehydration] = 0) to give

$$\Delta\Delta G_B^\circ = \Delta\Delta G_f^\circ[\text{metal-occupied protein}] + \Delta\Delta G_f^\circ[\text{released water}] + \Delta\Delta G_f^\circ[\text{released protons}] - \Delta\Delta G_f^\circ[\text{apo-protein}] \quad (5)$$

Equation 5 shows that when two sites release similar numbers of water molecules and protons upon the binding of the same metal, the overall $\Delta\Delta G_B^\circ$ is now dominated by the stability differences between the apo- and metal-occupied states of the two proteins. Moreover, the apo-states of the two sites are metal-independent. Thus, the overall shapes of the ionic selectivity profiles observed for different sites (see Figures 2 and 3 below) will be the same unless their metal-occupied states differ in their details of metal-site interactions or solvation. It follows that the different *shapes* observed for different mutants can be attributed fully to the contrasting features of their metal-occupied sites.

Molecular Graphics. Molecular images were displayed using Insight II graphics software (Biosym, v. 2.3.5) running on a Silicon Graphics Personal Iris 4D/35. Structural coordinates were retrieved from the Brookhaven Protein Data Bank (PDB). Backbone ϕ,ψ angles were measured by the PDB Analysis Program, version 1.3 (Chervitz and Falke, unpublished).

RESULTS

Construction of Engineered Proteins. Wild type GBP possesses a single intrinsic Gly residue at EF-loop position 6. The present study utilizes this protein as well as the eleven Gly variants listed in Table 2. In eight of the eleven variants (D134G, L135G, N136G, K137G, D138G, Q140G, I141G, and Q142G), a second Gly was introduced by site-directed mutagenesis at one of loop positions 1−5 or 7−9; similarly, a ninth variant (E205G) added a second Gly by replacing the coordinating Glu outside the EF-loop. The tenth variant (G139N) replaced the intrinsic Gly at position 6 with Asn, the second most common residue at this position in natural EF-loops (Kawasaki & Kretsinger, 1994), yielding an EF-loop lacking Gly entirely. The final eleventh variant, a double mutant (G139N, Q140G), replaced the intrinsic Gly with Asn and, at the same time, introduced Gly at the adjacent position 7. Of the eleven variants, two were previously described (K137G and Q142G), while the remaining nine were constructed for this study by site-directed mutagenesis of the GBP gene in plasmid pSF5 (Drake & Falke, 1996; Falke et al., 1991). For comparison, six additional control variants were included in the present study to illustrate the effects of non-Glu substitutions at coordinating side chain positions 3 and 9 (N136S, N136T, Q142N, Q142S, Q142T, Q142A). The construction of the latter proteins is described elsewhere (Drake et al., 1997; Drake & Falke, 1996).

Expression and Isolation of Engineered Proteins. The engineered genes encoding Gly variants were tested for expression in growth media containing 1 mM $MgCl_2$, $CaCl_2$, and $SrCl_2$ to maximize the occupancy of the GBP metal binding site. As summarized in Table 2, Gly variants at the non-coordinating EF-loop positions 2, 4, and 6 yielded normal expression levels of stable protein (L135G, K137G, G139N), as did Gly substitutions at coordinating positions 7 and 9 (Q140G, Q142G). The side chains of the latter two positions are not required for metal coordination, since position 7 provides coordination via its backbone carbonyl oxygen, while removal of the coordinating Glu side chain at position 9 results in axial coordination by a solvent molecule (Quiocho, Villa, and Falke, in preparation; Strynadka & James, 1989). By contrast, protein expression was lost when Gly substitution removed an essential coordinating side chain at loop position 1, 3, or 5 or at the final coordinating position outside the loop (D134G, N136G, D138G, E205G). Similarly, protein expression was blocked by Gly substitution for the buried Ile side chain at position 8 (I141G), which stabilizes the folded conformation of the EF-loop (Falke et al., 1994; Strynadka & James, 1989). These results suggest that, as previously observed in other studies, sites which fail to bind a divalent cation yield protein destabilization and degradation of GBP in the proteolytic environment of the periplasm (Drake & Falke, 1996; Drake et al., 1997). Such

results are consistent with the known structural role of the GBP Ca^{2+} binding site in the stabilization of the folded protein (Vyas et al., 1987).

The six viable Gly variants were expressed and purified by standard methods to greater than 90% purity as judged by SDS−PAGE gel electrophoresis (Drake & Falke, 1996). Their expected molecular masses were confirmed by quadropole electrospray mass spectrometry, as shown in Table 2. The viable proteins were L135G, K137G, G139N, Q140G, G139N/Q140G, and Q142G, which were subjected to further analyses in parallel to enable direct, side-by-side comparisons. The six non-Gly substitutions at EF-loop positions 3 and 9 (see above) also yielded stable, viable proteins which were purified and confirmed by mass spectrometry in the same fashion described for the Gly variants (Drake et al., 1997; Drake & Falke, 1996).

Engineered Protein Characterization. The stabilities of the six isolated Gly variants were compared to wild type in a thermal unfolding assay, which monitored the intrinsic fluorescence of the five GBP Trp residues. Each of these mutants gave a sharp melting curve and a T_m value within 6 °C of that of the native protein, as summarized in Table 2. Three of the Gly substitutions, K137G, G139N, and Q140G, yielded T_m values only slightly lower (−0.4 to −2.2 °C) than wild type. In contrast, the L135G, G139N/Q140G, and Q142G substitutions decreased T_m by a significantly greater extent (−5 to −7 °C), indicating that they caused greater destabilization. Yet even these substitutions retained T_m values exceeding 50 °C, demonstrating that all of the expressed Gly variants were stable and well-folded.

Complementary information regarding the stability and functionality of Gly variants was provided by equilibrium sugar binding measurements. Each of the viable mutants was found to retain high-affinity D-galactose binding, often binding ligand more tightly than wild type. Table 2 shows that the G139N, Q140G, and Q142G substitutions enhanced the D-galactose affinity approximately 3-fold while the L135G, K137G, and G139N/Q140G substitutions had little or no effect. Such results provide additional evidence that the six Gly variants were stable, functional proteins. Similarly, the six non-Gly mutations at EF-hand loop positions 3 and 9 lowered T_m by less than −7 °C and altered the D-galactose affinity by less than 2-fold, so that these mutants were also stable and functional (Drake et al., 1997; Drake & Falke, 1996).

Metal Binding Measurements. As in our previous studies of GBP, the phosphorescent lanthanide Tb^{3+} was used as a probe cation in studies of metal binding (Falke et al., 1991; Drake & Falke, 1996; Drake et al., 1996a). Numerous laboratories have shown that Tb^{3+} is a functional replacement for Ca^{2+} in EF-hands (Burroughs et al., 1994; Horrocks, 1993; Horrocks & Albin, 1984; Brittain et al., 1976; Moews & Kretsinger, 1975) because Tb^{3+} and Ca^{2+} both possess spherical, filled outer electronic subshells and are similar in size [their effective ionic radii for 7-fold coordination are 0.98 and 1.06 Å, respectively (Shannon, 1976)]. In the GBP site, Trp127 is located within 5 Å of the bound metal ion and thus can be used to excite a bound Tb^{3+} ion by energy transfer, thereby providing the basis for a sensitive fluorescence assay for Tb^{3+} occupancy of the GBP site (Snyder et al., 1990). Since only the bound, not the free, Tb^{3+} is excited by energy transfer from Trp127, the detected Tb^{3+} emission emanates solely from the bound metal population of interest. Using this approach, the equilibrium and kinetics of Tb^{3+} binding can be directly measured while the equilibrium binding of other metals can be quantified by their competitive displacement of Tb^{3+}.

Table 3: Effects of Ca^{2+} Binding Loop Substitutions on Metal Binding and Dissociation[a]

position	site	$k_{off}(Tb^{3+})$ (s^{-1})	$K_D(Tb^{3+})$ (μM)	$K_D(Ca^{2+})$ (μM)
X	WT	$(6.41 \pm 0.03) \times 10^{-3}$	3.0 ± 0.9	1.6 ± 0.4
2	L135G	$(7.36 \pm 0.04) \times 10^{-1}$	5.3 ± 0.4	3.3 ± 0.1
3	N136S[b]	$(8.46 \pm 0.09) \times 10^{-2}$	0.7 ± 0.1	3.7 ± 0.5
3	N136T[b]	$(9.28 \pm 0.06) \times 10^{-2}$	0.6 ± 0.1	13.3 ± 0.9
4	K137G	$(6.34 \pm 0.03) \times 10^{-3}$	1.8 ± 0.2	0.9 ± 0.1
6	G139N	$(3.17 \pm 0.01) \times 10^{-2}$	3.1 ± 0.9	2.1 ± 0.1
6/7	G139N/Q140G	$(4.61 \pm 0.03) \times 10^{-1}$	6.2 ± 0.9	3.2 ± 0.1
7	Q140G	$(1.16 \pm 0.01) \times 10^{-1}$	4.0 ± 0.2	2.1 ± 0.1
9	Q142G	$(2.00 \pm 0.05) \times 10^{0}$	1.4 ± 0.4	0.4 ± 0.1
9	Q142S[c]	$(6.50 \pm 0.09) \times 10^{-1}$	0.8 ± 0.1	0.7 ± 0.1
9	Q142T[c]	$(9.10 \pm 0.30) \times 10^{-1}$	2.3 ± 0.2	3.6 ± 0.1
9	Q142N[c]	$(1.02 \pm 0.03) \times 10^{0}$	1.9 ± 0.3	0.7 ± 0.1
9	Q142A[c]	$(3.97 \pm 0.08) \times 10^{0}$	2.8 ± 0.2	1.2 ± 0.1

[a] Errors are standard deviations for $n \geq 7$. [b] From Drake et al. (1997). [c] From Drake and Falke (1996) and Drake et al. (1996).

Metal Ion Affinities. Table 3 summarizes the Tb^{3+} and Ca^{2+} affinities of the wild type and engineered proteins. The Tb^{3+} and Ca^{2+} dissociation constants (K_D) of the six stable Gly variants (L135G, K137G, G139N, Q140G, G139N/Q140G, Q142G) were found to differ only 4-fold or less from the wild type values. It follows that the equilibrium Tb^{3+} and Ca^{2+} affinities were relatively insensitive to changes in backbone torsional constraints at each of EF-loop positions 2, 4, 6, 7, and 9.

In contrast to the minor affinity changes observed for the six stable Gly variants, Gly incorporation at loop positions 1, 3, 5, and 8 as well as at the external coordinating position (D134G, N136G, D138G, I141G, E205G) blocked protein expression in 1 mM Mg^{2+}, Ca^{2+}, and Sr^{2+}, as described above. Each of these Gly substitutions destabilizes the protein, most likely by a catastrophic reduction of the metal binding affinity. Such dramatic effects can be attributed to the loss of a coordinating side chain (loop positions 1, 3, and 5 and external) or a hydrophobic side chain required for loop stability (position 8). Table 3 indicates that more conservative non-Gly substitutions at coordinating positions 3 and 9 (N136S, N136T, Q142S, Q142T, Q142N, Q142A) retain Tb^{3+} and Ca^{2+} binding, although moderate changes to the metal binding affinities are sometimes observed (Drake et al., 1996, 1997; Drake & Falke, 1996). For example, the N136T substitution reduces the Ca^{2+} affinity 8-fold relative to wild type (Table 3).

Metal Ion Selectivities. In order to systematically analyze and compare the equilibrium metal binding parameters of the wild type and engineered GBP proteins, the affinities of each protein were measured for a pool of 20 spherical metal ions differing in size and charge, namely, selected spherical cations of groups Ia, IIa, and IIIa and the lanthanides (Snyder et al., 1990). The six stable Gly mutants exhibited the same ionic charge selectivity as wild type, as did the six non-Gly substitutions at coordinating positions 3 and 9: in every case, the altered Ca^{2+} binding site excluded monovalent cations while divalent and trivalent ions were bound with affinities that depend on their sizes.

To quantitate the ionic size selectivity of each site, the spherical metal ions were used to generate size selectivity

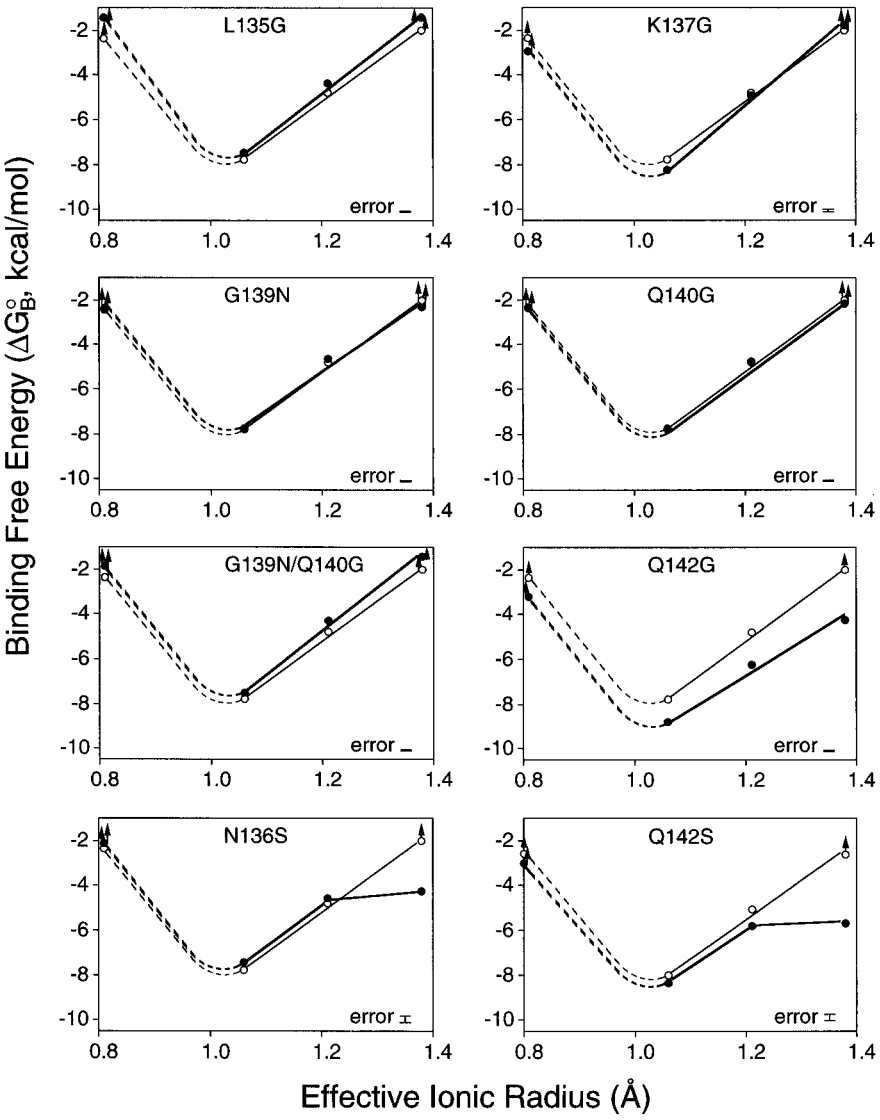

FIGURE 3: Binding free energy as a function of divalent cation size: effect of Gly and coordinating side chain substitutions. Plotted are the binding free energies for divalent cations of group IIa against the effective ionic radius of these metal ions (Shannon, 1976; 7-fold coordination). Each panel shows data for an engineered site (filled circles, bold curve) superimposed on the data for the native site (open circles, fine curve). The error bar in the lower right corner of each panel indicates the largest error in each data set, calculated as $RT \ln(K_D \pm 1$ standard deviation). Group IIa cations utilized were, in order of increasing radius, Mg^{2+}, Ca^{2+}, Sr^{2+}, and Ba^{2+}. Dashed curves indicate regions of the free energy profile which are incompletely determined by the available radii. Lower limits (up arrows) are indicated for ions which yielded less than 50% displacement of Tb^{3+} at their maximum attainable concentrations in the Tb^{3+} competition assay. All measurements were at 25 °C with 2.5 μM protein, 100 mM KCl, and 10 mM PIPES, pH 6.0.

profiles in which the free energies of binding were plotted versus the effective ionic radii of the metal ion substrates. Figures 3 and 4 illustrate the resulting size selectivity profiles for divalent and trivalent ions respectively. In each profile, the free energy minimum indicates the optimal or preferred ionic radius, while the slope defines the size selectivity of the site. The different *shapes* sometimes observed for the size selectivity profiles of different mutants can be fully attributed to the contrasting free energies of their metal-occupied states, since the apo-state of each protein contributes a constant free energy term that is independent of metal ion (see eq 5 in Methods). The most dramatic shape differences were observed between the Gly variants at non-coordinating side chain positions and the mutations at positions 3 and 9, which highlighted the more dramatic effects generated by the replacement of a coordinating side chain.

For divalent cations, the size selectivity profiles of the Gly variants in Figure 3 were nearly identical to wild type, with the exception of the Q142G substitution at EF-loop position 9. The latter mutant bound all divalent ions significantly more tightly than wild type. Notably, this Q142G mutation is also the only stable Gly substitution which removes a coordinating side chain, yielding coordination by a solvent oxygen at this position (Strynadka & James, 1989). For comparison, the size selectivity profiles of the more conservative N136S and Q142S coordinating side chain substitutions are also shown (Figure 3). These coordinating side chain substitutions, like Q142G, altered the size selectivity profile for divalent cations to a significantly greater extent than Gly substitutions at non-coordinating positions.

A similar, but even more striking, pattern of effects was revealed by the size selectivity profiles for spherical trivalent cations, as illustrated in Figure 4. Again, the five stable Gly variants at non-coordinating side chain positions yielded little or no effect on the ionic size selectivity, while the N136S, Q142S, and Q142G substitutions at coordinating positions 3 and 9 yielded dramatic changes. The latter three substitutions each significantly shifted the optimal size to larger ionic

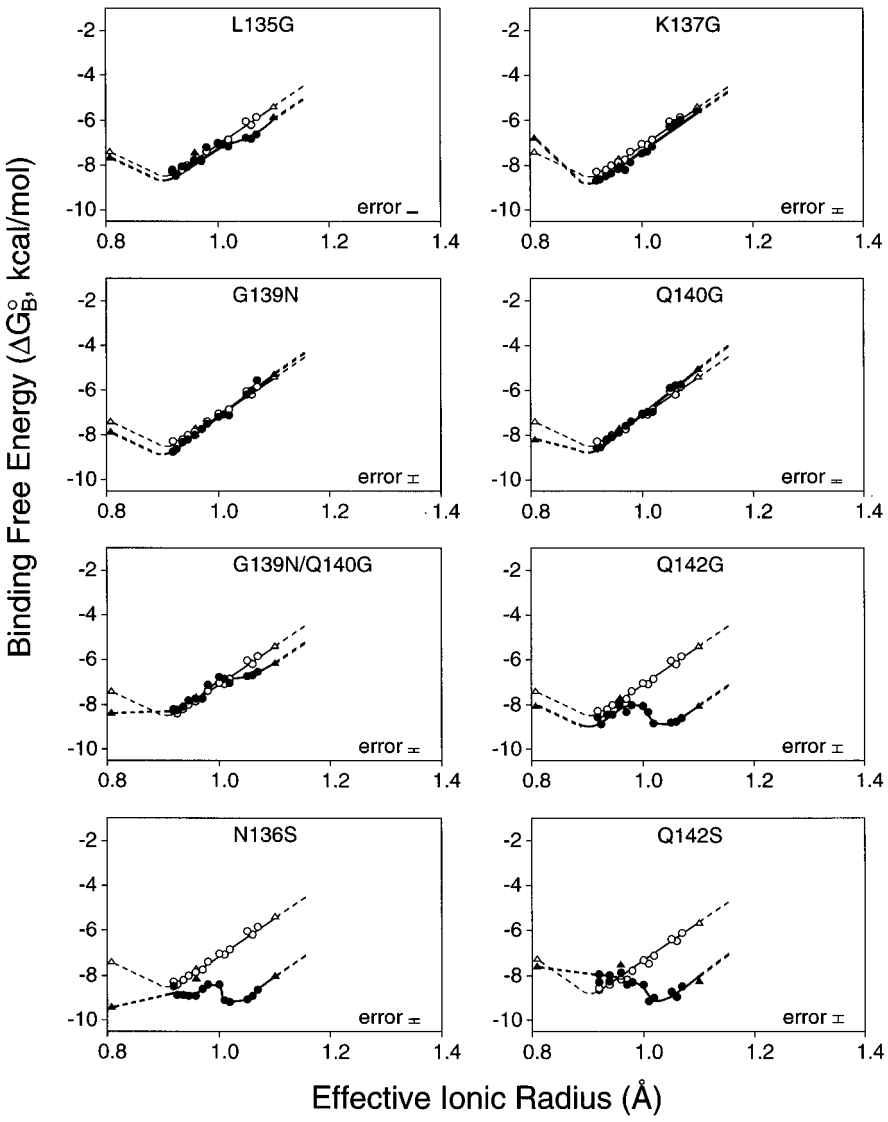

FIGURE 4: Binding free energy as a function of trivalent cation size: effect of Gly and coordinating side chain substitutions. Legend as for Figure 3, except that the indicated binding free energies are for trivalent cations from group IIIa (triangles) and the lanthanides (circles). In order of increasing radius, these were Sc^{3+}, Lu^{3+}, Yb^{3+}, Tm^{3+}, Er^{3+}, Ho^{3+}, Y^{3+}, Dy^{3+}, Tb^{3+}, Gd^{3+}, Eu^{3+}, Sm^{3+}, Nd^{3+}, Pr^{3+}, Ce^{3+}, and La^{3+}.

radius. Moreover, these substitutions enhanced the binding affinities of large cations, thereby flattening the size selectivity profile and decreasing the overall ability of the site to discriminate between metal ions of different size. Significantly, the effects of the Q142S substitution on size selectivity are quite similar to those observed for Q142G (Figure 4). It follows that most of the effects of the Q142G substitution on size selectivity arise from the replacement of a coordinating side chain, not from the effect of an engineered Gly on backbone torsion angle constraints. Nearly identical effects have been seen for all eight of the isoelectric side chain substitutions characterized at loop positions 3 and 9 (N136S, N136Q, N136V, N136T, Q142S, Q142N, Q142T, Q142A; Drake et al., 1996, 1997). Thus, in general, Gly variants at EF-loop positions 2, 4, 6, and 7 yielded quite small effects on ionic size selectivity, especially when compared to the eight isoelectric replacements of the coordinating side chains at loop positions 3 and 9 (Drake et al., 1996, 1997).

Metal Ion Dissociation Rates. While technical factors have prevented the measurement of Ca^{2+} dissociation rates from GBP and its mutants (Drake & Falke, 1996), the rates of Tb^{3+} dissociation are conveniently measured by the intrinsic Trp to Tb^{3+} energy transfer assay. Table 3 summarizes the Tb^{3+} dissociation rates of the viable Gly mutants, and, for comparison, the rates for the non-Gly substitutions at coordinating positions 3 and 9 (Drake et al., 1997; Drake & Falke, 1996). Gly substitutions at positions 2, 4, 6, and 7 yielded Tb^{3+} dissociation rates indistinguishable from wild type (K137G) or somewhat faster than wild type (L135G, G139N, G139N/Q140G, Q140G). The largest effect was produced by the L135G substitution at position 2, which increased the Tb^{3+} dissociation rate 110-fold. This enhancement of Tb^{3+} dissociation kinetics arose primarily from a lowering of the activation barrier for metal binding and release, since both the on- and off-rates were increased by similar factors to yield a nearly wild type Tb^{3+} affinity. Even the largest kinetic effects observed for Gly and position 3 substitutions were, however, considerably smaller than those observed for substitutions at position 9, termed the gateway position (Drake & Falke, 1996), where Tb^{3+} dissociation is speeded up to 620-fold by the Q142A substitution (Table 3). Thus substitutions at the gateway coordinating position yield larger kinetic effects than ob-

served for (i) substitutions at a different coordinating side chain position or (ii) Gly substitutions which alter the backbone torsion angle constraints at the non-coordinating side chain positions 2, 4, 6, and 7.

DISCUSSION

The Gly substitutions examined in this study significantly alter the range of allowed torsion angles available to the GBP Ca^{2+} chelation loop. In principle, these Gly variants could alter the thermal dynamics, entropy, and stiffness of the loop. The above results demonstrate that Gly or other substitutions which alter essential coordinating or hydrophobic side chains at loop position 1, 3, 5, 8, or 9 substantially perturb GBP stability or its metal binding parameters, while Gly variants at non-coordinating loop positions often yield surprisingly minor effects. These findings have significant implications for the molecular mechanisms used to tune the metal binding affinity, selectivity, and kinetics of the GBP Ca^{2+} chelation loop, as well as the closely related EF-loops of EF-hand proteins.

Gly incorporation into the GBP loop at position 2, 4, or 7, as well as removal of Gly at position 6, is found to have little effect on the affinities for Ca^{2+}, Tb^{3+}, and eighteen other spherical metal ions (Table 3). The observation that these Gly substitutions fail to substantially alter the metal binding equilibria suggests that Gly at these positions does not change the ΔS_o for metal binding to the loop. In this scenario, either Gly does not significantly affect the entropy of the loop in its apo- and metal-occupied states or it alters the entropy of these two states in a similar way. An alternative explanation is that the Gly substitutions alter both ΔH_o and ΔS_o for metal binding such that these enthalpic and entropic effects fortuitously cancel. In the present case such fortuitous cancellation seems highly unlikely since it would have to occur for the binding of twenty different metal ions differing in size and charge to five different Gly variants.

These same Gly variants at loop positions 2, 4, 6, and 7 also exhibit nearly wild type metal binding selectivities, operationally defined as the ability to discriminate between twenty different spherical metal cations of groups Ia, IIa, and IIIa and the lanthanides (Figures 3 and 4). It follows that the ionic size selectivity of the Ca^{2+} binding loop is not controlled by backbone torsion angle constraints at these four loop positions, each of which should modulate the resistance of the loop toward certain types of backbone displacements. Thus, if constraints on the loop backbone structure are important to ionic size selectivity, these constraints must be provided by other structural features outside the loop. Such alternative structural constraints might include (i) the fixed ends of the loop provided by the protein framework, (ii) hydrophobic contacts by loop side chains, such as Ile at position 8, and (iii) the intra-site hydrogen bonding network which includes backbone carbonyl and amide moieties (Strynadka & James, 1989). In contrast to the minor effects observed for the non-coordinating Gly substitutions, eight different substitutions altering the coordinating side chains at loop positions 3 and 9 all significantly perturb the ionic size selectivity in similar ways [Figures 3 and 4; also Drake et al. (1996, 1997)]. Together these results support the coordination cage model of ionic size selectivity, in which specific contacts between multiple coordinating side chains provide a highly constrained metal binding cavity with an optimal radius (Drake et al., 1996, 1997). In this model, substitution of a coordinating side chain disrupts the network of interactions constraining the cavity, thereby increasing the ability of the site to bind ions of different size, as observed. The external bidentate side chain may play an especially important role in the discrimination between Ca^{2+} and Mg^{2+} (DaSilva et al., 1995). Torsion angle constraints within the loop backbone, specifically at positions 2, 4, 6, and 7, do not directly define the size of the metal binding cavity.

Gly substitutions often measurably speed the rate of metal binding and release, confirming that they enhance certain types of loop dynamics. While Gly incorporation at position 4 retains the wild type rates of Tb^{3+} binding and release, Gly variants at positions 2, 6, and 7 exhibit increased Tb^{3+} binding and dissociation rates. In the latter cases the Tb^{3+} on- and off-rates are altered by similar factors so that the equilibrium Tb^{3+} is not substantially changed. Moderate kinetic enhancements of ~100-fold and ~20-fold are observed for Gly incorporation at loop positions 2 and 7, respectively. In natural EF-hand sites Gly is found only rarely (<2%) at these positions (Table 1), indicating that such Gly residues are not often used to tune the metal binding kinetics of the EF-loop. The largest kinetic effects, however, are observed for Gly and other substitutions at the gateway position 9, which provides axial side chain coordination in the wild type site. These results are consistent with the gateway model for kinetic tuning, in which the rate of metal binding and release is controlled by the gateway side chain at this loop position (Drake & Falke, 1996). Both in the GBP site and classical EF-hand sites, the gateway side chain blocks the shortest pathway between the metal binding cavity and solvent, thereby modulating the kinetics of access between the site and solution. The present findings (Table 3) and previous results (Drake & Falke 1996; Drake et al., 1997) indicate that side chains shorter than the native Gln at the gateway position increase Tb^{3+} on- and off-rates substantially more than (i) Gly substitutions within the loop and (ii) coordinating side chain substitutions at other loop positions. Moreover, a strong correlation is observed between function and the identity of the gateway side chain in natural sites: in slow structural or buffering sites such as the GBP site or site I of the parvalbumins, a long gateway side chain (Gln or Glu) is used to provide direct Ca^{2+} coordination and the maximum steric block (Figure 1). In the rapid signaling sites of calmodulin and troponin C, by contrast, a shorter gateway side chain is used, yielding solvent coordination at this axial position and minimal steric block to binding and dissociation. Such gateway tuning is one of the fundamental mechanisms used to modulate the lifetime of the Ca^{2+}-activated state in signaling proteins. Other important mechanisms the include intermolecular interactions between a signaling protein such as calmodulin and its target enzymes (Peersen et al., 1997; Bayley et al., 1996; Johnson et al., 1996).

One particularly surprising result of the present study is that despite the widespread usage of Gly at loop position 6 in GBP and most EF-hand sites, this residue does not contribute substantially to the equilibrium metal binding affinity and selectivity and has only a small effect (less than 5-fold) on the metal binding kinetics (Table 3; Figures 3 and 4). These findings imply that the conserved Gly must play an important role in some other capacity. In EF-hand Ca^{2+} signaling proteins of the calmoduling and troponin C

superfamilies, the Gly at position 6 has been proposed to serve as an intra-loop hinge (Falke et al., 1994) which facilitates relative movements of the terminal helices during the Ca^{2+}-triggered conformational rearrangement required for effector protein regulation [Finn et al., 1995; Gagné et al., 1995; Kuboniwa et al., 1995; reviewed by Ikura (1996)]. Alternatively, the Gly at position 6 could simply enhance protein stability as demonstrated for the GBP site in the present study, presumably due to the unusual torsion angle requirements of the backbone fold at this loop position (see Figure 2C). If, moreover, the stabilities of the apo- and metal-occupied states were affected in a similar fashion, the Gly residue would have little effect on metal binding equilibria, as observed. Further studies are needed to resolve this issue. Overall, however, the available results are consistent with a model in which the coordinating side chains dominate the metal binding parameters of the EF-loop, while intrinsic Gly residues play other roles related to loop stabilization or Ca^{2+}-induced structural changes.

ACKNOWLEDGMENT

The authors thank Drs. Craig Kundrot, Paul Melançon, Natalie Ahn, Olve Peersen, Andrea Hazard, and Eric Nalefski for helpful discussions and the NIH for funding (GM48203 to J.J.F.).

REFERENCES

Bayley, P. M., Findlay, W. A., & Martin, S. R. (1996) *Protein Sci. 5*, 1215−1228.
Brittain, H. G., Richardson, F. S., & Martin, R. B. (1976) *J. Am. Chem. Soc. 98*, 8255−8260.
Burroughs, S. E., Horrocks, W. D., Ren, H., & Klee, C. B. (1994) *Biochemistry 33*, 10428−10436.
Carafoli, E., Garciamartin, E. & Guerini, D. (1996) *Experentia 52*, 1091−1100.
Chattopadhyaya, R., Meador, W. E., Means, A. R. & Quiocho, F. A. (1992) *J. Mol. Biol. 228*, 1177−1192.
Chen, X.-H., Bezprozvanny, I. & Tsien, R. W. (1996) *J. Gen. Physiol. 108*, 363−374.
Creighton, T. E. (1993) *Proteins* W. H. Freeman & Co., New York.
DaSilva, A. C. R., Kendrick-Jones, J., & Reinach, F. C. (1995) *J. Biol. Chem. 270*, 6773−6778.
Drake, S. K., & Falke, J. J. (1996) *Biochemistry 35*, 1753−1760.
Drake, S. K., Lee, K. L., & Falke, J. J. (1996) *Biochemistry 35*, 6697−6705.
Drake, S. K., Zimmer, M. A., Kundrot, C., & Falke, J. J. (1997) *J. Gen. Physiol.*, submitted.
Ellinor, P. T., Yang, J., Sather, W. A., Zhang, J. F., & Tsien, R. W. (1995) *Neuron 15*, 1121−1132.
Falke, J. J., Snyder, E. E., Thatcher, K. C., & Voertler, C. S. (1991) *Biochemistry 30*, 8690−8697.
Falke, J. J., Drake, S. K., Hazard, A. L., & Peersen, O. B. (1994) *Q. Rev. Biophys. 27*, 219−290.
Finn, B. E., Evenas, J., Drakenberg, T., Waltho, J. P., Thulin, E., & Forsén, S. (1995) *Nature Struct. Biol. 2*, 777−783.
Gagné, S. M., Tsuda, S., Li, M. X., Smillie, L. B., & Sykes, B. D. (1995) *Nat. Struct. Biol. 2*, 784−789.
Horrocks, W. D. (1993) *Methods Enzymol. 226*, 495−538.
Ikura, M. (1996) *Trends Biol. Sci. 21*, 14−17.
Innis, M. A., Myambo, K. B., Gelfand, D. H., & Brow, M. A. D. (1988) *Proc. Natl. Acad. Sci. U.S.A. 85*, 9436−9440.
Johnson, J. D., Snyder, C., Walsh, M., & Flynn M. (1996) *J. Biol. Chem. 271*, 761−767.
Kawasaki, H., & Kretsinger, R. H. (1994) *Protein Profiles 1*, 343−517.
Kretsinger, R. H., & Nockolds, C. E. (1973) *J. Biol. Chem. 248*, 3313−3326.
Kuboniwa, H., Tjandra, N., Grzesiek, S., Ren, H., Klee, C. B., & Bax, A. (1995) *Nat. Struct. Biol. 2*, 768−776.
Kunkel, T. A., Roberts, J. D., & Zakour, R. A. (1987) *Methods Enzymol. 154*, 367−382.
Linse, S., & Forsén, S. (1995) *Adv. Second Messenger Phosphoprotein Res. 30*, 89−151.
Marsden, B. J., Shaw, G. S., & Sykes, B. D. (1990) *Biochem. Cell Biol. 68*, 587−601.
Miller, C. (1996) *J. Gen. Physiol. 107*, 445−447.
Moews, P. C., & Kretsinger, R. H. (1975) *J. Mol. Biol. 91*, 229−232.
Park, C. S., & MacKinnon, R. (1995) *Biochemistry 34*, 13328−13333.
Renner, M., Danielson, M. A., & Falke, J. J. (1993) *Proc. Natl. Acad. Sci. U.S.A. 90*, 6493−6497.
Schwarzenbach, G. (1952) *Helv. Chim. Acta 35*, 2344−2359.
Shannon, R. D. (1976) *Acta Crystallogr. A 32*, 751−767.
Skelton, N. J., Kördel, J., Akke, M., Forsén, S., & Chazin, W. J. (1994) *Nat. Struct. Biol. 1*, 239−245.
Snyder, E. E., Buoscio, B. W., & Falke, J. J. (1990) *Biochemistry 29*, 3937−3943.
Strynadka, N. C. J., & James, M. N. G. (1989) *Annu. Rev. Biochem. 58*, 951−998.
Vyas, N. K., Vyas, M. N., & Quiocho, F. A. (1987) *Nature 327*, 635−638.

BI9703913